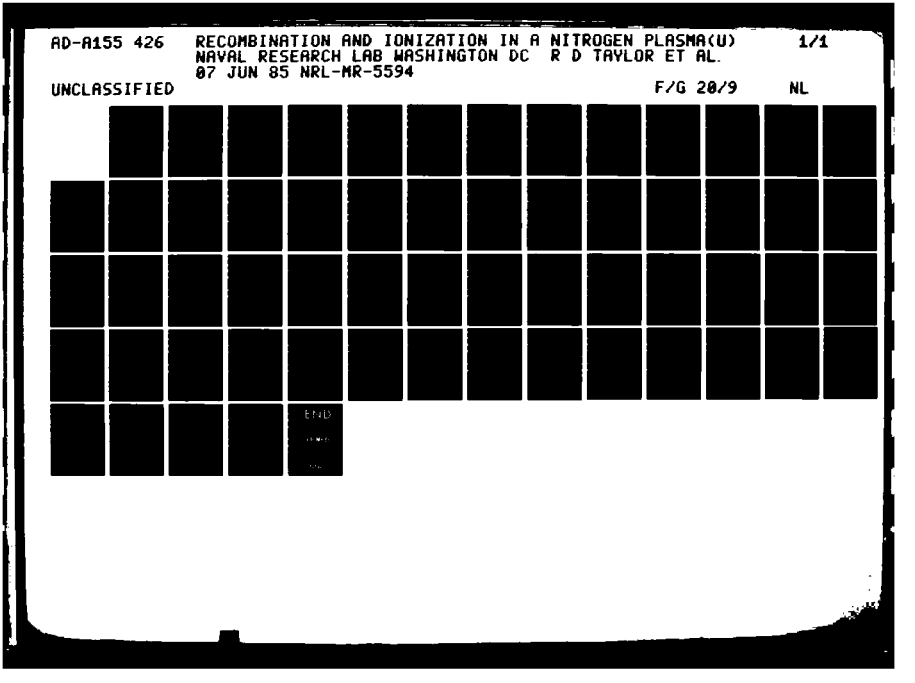
AD-A155 426 RECOMBINATION AND IONIZATION IN A NITROGEN PLASMA(U) 1/1
NAVAL RESEARCH LAB WASHINGTON DC R D TAYLOR ET AL.
07 JUN 85 NRL-MR-5594
UNCLASSIFIED F/G 20/9 NL
END

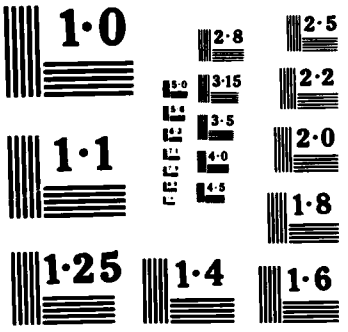

NATIONAL BUREAU OF STANDARDS
MICROCOPY RESOLUTION TEST CHART

NRL Memorandum Report 5594

Recombination and Ionization in a Nitrogen Plasma

R. D. TAYLOR

Berkeley Research Associates
Springfield, VA 22150

A. W. ALI

Plasma Physics Division

June 7, 1985

This report was supported by the Defense Advanced Research Projects Agency (DoD), ARPA Order No. 4395, Amendment No. 54, monitored by the Naval Surface Weapons Center under Contract No. N60921-85-WR-W0131.

NAVAL RESEARCH LABORATORY
Washington, D.C.

SECURITY CLASSIFICATION OF THIS PAGE

REPORT DOCUMENTATION PAGE

1a REPORT SECURITY CLASSIFICATION UNCLASSIFIED	1b RESTRICTIVE MARKINGS
2a SECURITY CLASSIFICATION AUTHORITY	3 DISTRIBUTION/AVAILABILITY OF REPORT Approved for public release; distribution unlimited.
2b DECLASSIFICATION/DOWNGRADING SCHEDULE	
4 PERFORMING ORGANIZATION REPORT NUMBER(S) NRL Memorandum Report 5594	5 MONITORING ORGANIZATION REPORT NUMBER(S)
6a NAME OF PERFORMING ORGANIZATION Naval Research Laboratory	6b OFFICE SYMBOL (If applicable) Code 4700.1
6c ADDRESS (City, State, and ZIP Code) Washington, DC 20375-5000	7a NAME OF MONITORING ORGANIZATION Naval Surface Weapons Center
	7b ADDRESS (City, State, and ZIP Code) Silver Spring, MD 20910
8a NAME OF FUNDING/SPONSORING ORGANIZATION DARPA	8b OFFICE SYMBOL (If applicable)
8c ADDRESS (City, State, and ZIP Code) Arlington, VA 22209	9 PROCUREMENT INSTRUMENT IDENTIFICATION NUMBER
	10 SOURCE OF FUNDING NUMBERS

PROGRAM ELEMENT NO	PROJECT NO	TASK NO	WORK UNIT ACCESSION NO
62707E			DN680-415

11 TITLE (Include Security Classification)
Recombination and Ionization in a Nitrogen Plasma

12 PERSONAL AUTHOR(S)
Taylor, R.D.* and Ali, A.W.

13a TYPE OF REPORT	13b TIME COVERED	14 DATE OF REPORT (Year, Month, Day)	15 PAGE COUNT
Interim	FROM 1984 TO 1985	1985 June 7	59

16 SUPPLEMENTARY NOTATION
*Berkeley Research Associates, Springfield, VA 22150 (Continues)

17 COSATI CODES			18 SUBJECT TERMS (Continue on reverse if necessary and identify by block number)		
FIELD	GROUP	SUB-GROUP	Collisional-radiative model	Emissions	LTE and Non LTE
			Nitrogen plasma	Excited states	

19 ABSTRACT (Continue on reverse if necessary and identify by block number)

A collisional-radiative model for a nitrogen plasma (N, N^+ and N^{++}) has been developed. The results for an optically thin, and optically thick in uv lines, are presented. The approach taken in the model is to solve a time dependent set of rate equations for a large number of excited states of N and N^+ for a wide range of Te and Ne. The excited states of interest emit radiation in the ultraviolet, visible and infrared which could be used for air plasma channel diagnostics.

The model delineates the regimes in Te and Ne where the excited states are in LTE and when they deviate from LTE, and is developed as a building block for an extensive radiative transfer model for air.

20 DISTRIBUTION/AVAILABILITY OF ABSTRACT	21 ABSTRACT SECURITY CLASSIFICATION
☒ UNCLASSIFIED/UNLIMITED ☐ SAME AS RPT ☐ DTIC USERS	UNCLASSIFIED
22a NAME OF RESPONSIBLE INDIVIDUAL A. W. Ali	22b TELEPHONE (Include Area Code) (202) 767-3762
	22c OFFICE SYMBOL Code 4700.1

DD FORM 1473, 84 MAR 83 APR edition may be used until exhausted
All other editions are obsolete

SECURITY CLASSIFICATION OF THIS PAGE

16. SUPPLEMENTARY NOTATION (Continued)

This report was supported by the Defense Advanced Research Projects Agency (DoD), ARPA Order No. 4395, Amendment No. 54, monitored by the Naval Surface Weapons Center under Contract No. N60921-85-WR-W0131.

CONTENTS

RECOMBINATION AND IONIZATION IN A NITROGEN PLASMA

I. INTRODUCTION

When air is heated and is highly ionized, nitrogen and its ions become relatively abundant for electron temperatures of 1-3 e.v. Emissions from such air provide diagnostic information and play a role in cooling the heated channel. To describe such a channel one must therefore perform a radiative transfer calculation which requires a detailed knowledge of the air species including excited states. To provide this information, we develop as a first step, a collisional-radiative model for nitrogen and its ion.

It is well known that a recombining plasma is a source of radiation. The character of this radiation, line versus continuum emission and absorption or uv versus visible and infrared radiation, depends on detailed aspects of the plasma. In addition to species type important properties include electron density, electron temperature, and optical character (thin, thick, or optically thick in select spectral regions). To quantitatively describe the spectral character of radiation emitted from a plasma these properties must be incorporated in a model which accurately monitors the evolution of the plasma, determines the extent to which the plasma is or is not in equilibrium, and accounts for the radiative transfer accordingly. For example, in the simplest case of a plasma in local

Manuscript approved April 16, 1985.

thermodynamic equilibrium (LTE) the radiative transfer equation may be solved assuming Planck's function correctly represents the source radiation [1]. A more complete description, however, requires coupling the radiative transfer equations to the rate equations which provide the population densities of all bound and continuum states involved in the radiative and collisional processes of the specific plasma. The work presented in this paper is the initial step in constructing such a model.

A collisional-radiative model developed by Bates et. al. [2] has provided the framework for studies which give the excited state populations and their deviation from LTE for hydrogen and hydrogenic ions. Their theory is statistical in nature and treats the problem in a simple and tractable way. Effective collisional-radiative recombination and ionization coefficients are defined and determined from a knowledge of the rate coefficients for collisional excitation and ionization and the spontaneous transition probabilities, for the case of an optically thin plasma. The influence of self-absorption is then demonstrated for the special cases of a hydrogen plasma optically thick for various optical transitions. Their approach is to solve a coupled set of rate equations for the steady state values of excited state densities at fixed electron densities and temperatures, thereby showing the extent to which the excited state populations deviate from Saha equilibrium.

The work of Bates et. al. has motivated others to study the effects of collisional and radiative processes in plasmas. Drawin [3] has used more recent cross section information and recalculated the collisional-radiative recombination and ionization coefficients for hydrogen and hydrogenic plasmas analogous to Bates et. al., but within the context of a more general formalism. Park [4] has used the method of Bates to compute spectral line intensities for specific non-equilibrium conditions in a collision-dominant nitrogen plasma. Kulander [5] has also studied the spectral properties of radiation emitted from a non-equilibrium nitrogen plasma as well as the deviation from Saha equilibrium of the excited and ionized states of an optically thin plasma.

In the present work the focus is on an optically thin nitrogen plasma, however, unlike Bates and others we solve the time-dependent coupled rate equations explicitly, in a manner similar to the approach taken by Ali & Jones [6] to study recombination lasers in hydrogen and hydrogen like plasmas. The calculations are for a given electron temperature, but allow the electron density to evolve in time. As expected the population densities show an early transient behavior followed by a steady state, from which we calculate effective collisional-radiative recombination and ionization coefficients and compare the final state populations to those expected if Saha equilibrium conditions were satisfied. Our rate equations include the most

satisfied. Our rate equations include the most recent ionization, excitation, and recombination rate coefficients available, some of which are similiar to those used by Drawin [3] and Bates [2], and some are based on experimental data. Finally, we consider the case of a nitrogen plasma optically thick in specific uv bound-bound spectral lines.

II. COLLISIONAL AND RADIATIVE PROCESSES

The coupled rate equations which describe the evolution of the nitrogen plasma include the following collisional and radiative processes:

1. Collisional excitation - excitation of an upper electronic state by collisions of electrons with atoms (ions) in a lower state.

$$\begin{aligned} e + N(i) &\rightarrow N(j) + e \qquad j > i \qquad X(i,j) \\ e + N^+(p) &\rightarrow N^+(q) + e \qquad q > p \qquad X^+(p,q) \end{aligned} \tag{1}$$

2. Collisional de-excitation - the inverse of 1.

$$\begin{aligned} e + N(j) &\rightarrow N(i) + e \qquad j > i \qquad Y(j,i) \\ e + N^+(q) &\rightarrow N^+(p) + e \qquad q > p \qquad Y^+(q,p) \end{aligned} \tag{2}$$

3. Collisional ionization - ionization of atoms and ions

$$\begin{aligned} e + N(i) &\rightarrow e + e + N^+(p) \qquad S(i,p) \\ e + N^+(p) &\rightarrow e + e + N^{++}(u) \qquad S^+(p,u) \end{aligned} \tag{3}$$

4. Three body recombination - the inverse of 3.

$$\begin{aligned} e + e + N^+(p) &\rightarrow N(i) + e \qquad \alpha_3(p,i) \\ e + e + N^{++}(u) &\rightarrow N^+(p) + e \qquad \alpha_3^+(u,p) \end{aligned} \tag{4}$$

5. Radiative recombination.

$$\begin{aligned} e + N^+(p) &\rightarrow N(i) + h\nu \qquad \alpha_R(p,i) \\ e + N^{++}(u) &\rightarrow N^+(p) + h\nu \qquad \alpha_R^+(u,p) \end{aligned} \tag{5}$$

6. Spontaneous emission.

$$N(j) \rightarrow N(i) + h\nu \qquad j > i \qquad A(j,i)$$
$$N^{+}(q) \rightarrow N^{+}(p) + h\nu \qquad q > p \qquad A^{+}(q,p) \tag{6}$$

Since we are initially assuming a nitrogen plasma that is optically thin for all spectral regions photo-ionization and absorption have been excluded. These processes are accounted for most easily by describing photo-ionization as negative radiative recombination and absorption as negative spontaneous emission as was done by Drawin [3], and will be included in detail in a subsequent report.

III. RATE EQUATIONS AND RATE COEFFICIENTS

A. Coupled rate equations

Let $N^{z-1}(m)$ denote the population density of the $(z-1)$-th ion (or neutral if $z=1$) in the electronic state whose index is m, where it is understood that the density depends on time. The rate equation describing the evolution of this state subject to the collisional and radiative processes outlined in the previous section is given by

$$\begin{aligned}
\frac{dN}{dt}^{z-1}(m) = {} & Ne \Big[\sum_{\ell \le m-1} N^{z-1}(\ell)\, X^{z-1}(\ell,m) - N^{z-1}(m) \sum_{\ell \le m-1} Y^{z-1}(m,\ell) \Big] \\
& + Ne \Big[\sum_{n \ge m-1} N^{z-1}(n)\, Y^{z-1}(n,m) - N^{z-1}(m) \sum_{n \ge m-1} X^{z-1}(m,n) \Big] \\
& + Ne \Big[Ne \sum_{n} N^{z}(n) \alpha_3^{z-1}(n,m) + \sum_{n} N^{z}(n) \alpha_R^{z-1}(n,m) \Big] \\
& - Ne\, N^{z-1}(m) \sum_{n} S^{z-1}(m,n) \qquad (7) \\
& - Ne \Big[Ne\, N^{z-1}(m) \sum_{\ell} \alpha_3^{z-2}(m,\ell) + N^{z-1}(m) \sum_{\ell} \alpha_R^{z-2}(m,\ell) \Big] \\
& + Ne \sum_{\ell} N^{z-2}(\ell)\, S^{z-2}(\ell,m) \\
& + \sum_{n \ge m+1} N^{z-1}(n)\, A^{z-1}(n,m) - N^{z-1}(m) \sum_{\ell \le m-1} N^{z-1}(\ell)\, A^{z-1}(\ell,m)
\end{aligned}$$

where Ne is the electron density. The time history of all species is obtained by solving the set of equations constructed from equation (7) for all ions and neutrals in all states, whose indices are n, ℓ, and m.

B. Energy Level Model

We have chosen to study the nitrogen plasma for electron temperatures in the range of 1.0 e.v. to 3.0 e.v.. In this temperature range the important radiation is produced by constituents which are atomic or ionic. In our calculation we have included the lowest thirteen (13) levels for N I, the lowest seventeen levels for N II, and two effective levels for N III. Details are presented in Tables I through III; this information can be found in Weise [7]. We note that this model includes as a subset the levels for N I and N II used in Kulander's studies [5], as well as most of the N III levels. While not as comprehensive in describing N I as Park [4], we account for N II and N III which he fails to do, since his interest is in a region of lower electron densities and higher temperatures.

Within this model the important bound-bound radiative transitions are listed in Table IV; each transition is described by its wavelength, the number given by Weise [7], spectral character, transition index (for example, 7+ - 1+ denotes emission from the seventh to the first level in the ion N II), and transition energy. This table shows, for instance, that the

visible radiation comes largely from transitions in the ion N II. Therefore, one would expect this radiation to be important once electron temperatures become sufficiently high that these upper levels of N II are accessed.

The important free-bound radiative transitions are listed in Table V. These include all transitions for the corresponding ions considered by Kulander [5b]. While there is a large amount of uv radiation the radiative recombination from N^+ -> N(i) where $i \geq 7$ is a source of visible emission. This becomes the predominant source of visible radiation at lower electron densities and temperatures; such that the abundance of N II that is created resides in the ground state.

C. Rate Coefficients

The rate coefficients for the collision and radiation processes outlined in section II. and used in the rate equations, i.e. equations (7) were obtained from several sources.

1. Transitions amongst the levels of the ground state configurations of nitrogen (^4S, ^2D, ^2P) and nitrogen ion (^3P, ^1D, ^1S) are optically forbidden. Electron impact excitation coefficients for the transitions in N I were obtained from reference [8]. Transitions among the metastable states in N II were accounted for using the analytic

expressions for the de-excitation rate coefficients given in reference [8]. The reverse rate coefficients were obtained from detailed balance.

2. Collisional excitation rates of transitions which are optically allowed, see Table IV, are obtained using the following simple formula [9]:

$$X(m,n) = \frac{4.3 \times 10^{-6} f(n,m) \exp\{-E(n,m)/Te\}}{E(n,m)\ Te^{1/2}}\ \Psi(n,m) \qquad (8)$$

where $E(n,m) = E(n) - E(m)$, $m < n$, $f(n,m)$ is the oscillator strength, and

$$\Psi(n,m) = 0.2 \text{ for ions} \qquad (9)$$

$$\Psi(n,m) = \left(1.0+\frac{E(n,m)}{Te}\right)^{-1} \left\{\left(20.0+\frac{E(n,m)}{Te}\right)^{-1} + \ln\left[1.25\left(1.0+Te/E(n,m)\right)\right]\right\}$$

for neutrals

The de-excitation rates are calculated from detailed balance.

3. Collisional ionization from a specific level m to the appropriate level, n, of the next highest ion was obtained using the formula of Drawin [3],

$$S^{z-1}(m,n) = 2.38 \times 10^{-8} \frac{E_H^2}{\Delta E} \frac{f(m)\xi(m)}{(Te)^{1/2}}\ \Psi\left(\frac{\Delta E}{Te}, 1\right) \qquad (10)$$

where E_H is 13.59 e.v., ξ (m) the number of equivalent electrons, $\Delta E = E^z(n) - E^{z-1}(m)$, f(m) the oscillator strength, and z = 1 for neutrals and > 1 for ions. Ψ is given by

$$\Psi\left(\frac{\Delta E}{Te},1\right) = \int_{\Delta E/Te}^{\infty} dx \left(1-\frac{\Delta E}{Te}\right) \exp(-x) \ln\left(\frac{1.253x}{\Delta E/Te}\right) \quad (11)$$

where $\beta = 1+[(z-1)/(z+2)]$. The oscillator strength was chosen so that rate coefficients given by equation (11) matched closely the ionization data in Table VIII of reference [10] which is based on experimental cross sections for the ionization of nitrogen; our choice was f(m) = 0.2. The rate coefficient for three-body recombination, obtained from detailed balance, is

$$\alpha_3^{z-1}(n,m) = 1.66 \times 10^{-22} \frac{g^{z-1}(m)}{g^z(n)} \frac{S^{z-1}(m,n)}{Te^{3/2}} \exp\left(\frac{\Delta E}{Te}\right) \quad (12)$$

where $g^{z-1}(m)$ is the statistical weight of state m and $g^z(n)$ is the weight of the ionic state.

4. The rate coefficients for radiative recombination were obtained using the approximate formula of Bates [2], e.g.

$$\alpha_R^{z-1}(p,i) = 5.2 \times 10^{-14} \exp\left(\frac{\Delta E}{Te}\right) \left(\frac{\Delta E}{Te}\right)^{3/2} E_1\left(\frac{\Delta E}{Te}\right) \quad (13)$$

Here E_1 is the exponential integral

$$E_1\left(\frac{\Delta E}{Te}\right) = \int_1^{\infty} \frac{dx}{x} \exp\left(\frac{\Delta E}{Te} x\right) \quad (14)$$

For example, eq.(13) gives the rate coefficient for recombination of level p of N II to level i of N I, see II. 5., if z = 1.

5. Finally, the Einstein A coefficients for spontaneous emission were taken from Weise [7].

D. Ionization Potential Reduction

The ionization energy of an isolated atom or ion is different from one immersed in a plasma [11] and must be corrected accordingly. The net ionization potential reduction is due to energy released upon placing an electron-ion pair in a plasma; one of the consequences is that electrons occupying states which in an isolated atom would be bound now become unbound should the corrected ionization potential be less than the energy of the state. Our rate equations have been modified to account for this high electron density (low electron temperature) phenomenon.

At each step in the numerical integration of the rate equations, eqs. (7), the electron density and temperature are noted and the ionization potential reduction, ΔE_∞^{z-1}, calculated according to

$$\Delta E_\infty^{z-1} = 1.93 \times 10^{-10} \; z \left(\frac{Ne}{Te}\right)^{1/2} \qquad (15)$$

where ΔE_{∞}^{z-1}, and Te are in e.v. and Ne has units #/cm^3. Reducing the ionization potential an amount determined by eq. (15) has the effect of modifying the collisional ionization rate coefficient, eq. (10), as follows:

$$S_c^{z-1}(m,n) = S^{z-1}(m,n) \times \exp\{\Delta E_{\infty}^{z-1}/Te\} \qquad (16)$$

For example, in the extreme case of low temperature, Te = 1.0 e.v., and high electron density, Ne = 10^{19}/cm^3, the ionization rate increases by 84% so its effect can be substantial.

IV. NUMERICAL RESULTS

A. Time-Dependent Population Densities

Figures (1)- (10) show representative results obtained by integrating equations (7). Numerical integration was accomplished by using CHEMEQ, a routine specifically designed to solve stiff ordinary differential equations [12]. The initial conditions for this set of figures are Te = 2.0 e.v., N(1) = 4.0 x $10^{18}/cm^3$, Ne = $N^+(1)$ = 1.0 x $10^{17}/cm^3$ (i.e. charge neutrality), with all other population densities being set equal to zero (actually 1 x $10^4/cm^3$). The general behavior of the time-dependent solutions is as expected - an early transient behavior followed by rapid relaxation to a steady state. The relaxation time is on the order of 15 - 22 nsec. Such rapid relaxation led Bates et. al. [2] to solve for the excited state population densities using a steady state approximation.

In Figure (1) the total population densities of the electrons, neutrals, and ions are presented. At Te = 2.0 e.v. the number of N^{++} ions is negligible, i.e. approximately three orders of magnitude less than the neutrals. Consequently, the total number of electrons nearly equals the total number of N^+ ions which, in the steady state, exceeds the population of neutrals by a factor of three.

Examination of Figures (2) - (4) shows that most of the nitrogen population resides in the ground state and the metastable states, particularly the $^2D^o$ state. The levels which contribute to the emission of bound-bound uv radiation, N(4-6,13), are approximately equal in population to those which contribute to the emission of bound-bound ir radiation, N(8-12).

As in the case of N the ground and metastable states of N^+ are the more heavily populated, see Figures (5) - (7). Unlike N only $N^+(4)$ and $N^+(5)$, i.e. the first two excited states which emit bound-bound uv, are highly populated because of the low electron temperature. The rest of the uv and visible emitting levels are two orders of magnitude less than the N radiating levels. The population of the lower N^+ levels is important for the emmision of radiation resulting from radiative recombination, free-bound.

Figure (8) shows that the N^{++} ions that are created reside, as expected, predominately in the ground state.

While a direct comparison cannot be made with the results of Kulander [5a] our steady state populations are in qualitative agreement. The relative population of the major equilibrium species for Ne = $10^{16}/cm^3$ to $10^{19}/cm^3$ and Te = 1.0 e.v. to 2.0 e.v. follows the trend obtained by Kulander. At Te = 1.0 e.v. N(1) is the major species for Ne = $10^{16}/cm^3$ to $10^{19}/cm^3$ while at Te = 2.0 e.v. $N^+(1)$ predominates. At Te = 1.5 e.v.

$N^+(1)$ is the major species at lower electron densities ($10^{16}/cm^3$ - $10^{18}/cm^3$) while N(1) is at higher density ($10^{19}/cm^3$). Kulander also presents results on the distribution of population amongst species versus electron concentration. Again our results are in general agreement. Detailed aspects of our population distribution are discussed in section IV. C..

B. Collisional-Radiative Recombination-Ionization Coefficients

Bates et. al. [2] have defined effective recombination and ionization coefficients which account for the net effect of collisional ionization, three-body recombination, and radiative recombination in a very simple way. These coefficients have been tabulated exclusively for hydrogen and hydrogenic ion plasmas, [2] and [3]. In this section we define the effective coefficients analogous to Bates et. al. and present results for our optically thin nitrogen plasma as well as the case where all bound-bound uv lines are assumed to be optically thick.

Denoting α°_{CR}, and α^{+}_{CR} as the effective recombination coefficients for $N^+ \rightarrow N$ and $N^{++} \rightarrow N^+$ and S°_{CR} and S^{+}_{CR} as the effective ionization coefficients for the reverse processes the rate equations for N, N^+, N^{++}, and Ne may be written

$$\frac{dN}{dt} = Ne\ N^+\ \alpha^{\circ}_{CR} - Ne\ N\ S^{\circ}_{CR}$$

$$\frac{dN^+}{dt} = -Ne\ N^+\ \alpha^o_{CR} + Ne\ N\ S^o_{CR} + Ne\ N^{++}\ \alpha^+_{CR} - Ne\ N^+ S^+_{CR}$$

$$\frac{dN^{++}}{dt} = Ne\ N^+\ S^+_{CR} - Ne\ N^{++}\alpha^+_{CR} \qquad (17)$$

$$\frac{dNe}{dt} = Ne\ N\ S^o_{CR} + Ne\ N^+\ S^+_{CR} - Ne\ N^+\alpha^o_{CR} - Ne\ N^{++}\alpha^+_{CR}$$

Therefore, in terms of the detailed rate coefficients outlined in section II. α^o_{CR}, α^+_{CR}, S^o_{CR}, and S^+_{CR} are given by

$$\alpha^o_{CR} = \{Ne \sum_{p,i} \alpha_3(p,i)\ N^+(p) + \sum_{p,i} \alpha_R(p,i)\ N^+(p)\}/N^+$$

$$\alpha^+_{CR} = \{Ne \sum_{p,u} \alpha^+_3(u,p)\ N^{++}(u) + \sum_{p,i} \alpha^+_R\ (u,p)\ N^{++}(u)\}/N^{++} \qquad (18)$$

$$S^o_{CR} = \{ \sum_{i,p} N(i)\ S(i,p)\}/N$$

$$S^o_{CR} = \{ \sum_{p,u} N^+(p)\ S^+(p,u)\}/N^+$$

A quick check shows that these definitions satisfy the conditions for particle and charge conservation.

The coefficients defined in equations (17) and (18) are time-dependent, due to the time dependence of the contributing population densities; see Figs. (9) - (10). The steady state values are presented in Tables VI - IX as a function of the final electron density and electron temperature (Te was fixed throughout the integration). Close examination of these results reveals the following: At high electron densities the effective recombination coefficient is linearly proportional to Ne. This is due to the dominance of three-body recombination over radiative (two-body) recombination in this regime, Ne $\geq 10^{13}$ -

$10^{19}/cm^3$. For lower electron densities the opposite is true and the effective coefficient approaches the two-body value. The collisional-radiative ionization coefficients show a rapid rise for low electron densities ($Ne \leq 10^{16} - 10^{17}/cm^3$) and a much slower rise for higer densities ($Ne \geq 10^{18}/cm^3$). This is in contrast to the behavior of the coefficients of Drawin and Bates which show a saturation at high Ne. The density dependence in S^{o}_{CR} and S^{+}_{CR} at high Ne in our calculation comes from the correction discussed in section III. D.. The level-specific collisional ionization coefficients depend on Ne and Te in the manner of eq. (16); this carries through to the definition of S^{o}_{CR} and S^{+}_{CR} in eq. (18). Neither Drawin nor Bates included this correction.

The collisional-radiative coefficients in Tables VI and VIII can be loosely compared to the results of Bates .et. al. [2] and Drawin [3]. While there is no apriori expectation that the results should be in strict agreement, to the extent that a nitrogen plasma differs from a hydrogenic plasma, many of the rate coefficients were obtained using similiar (hydrogenic) expressions. However, it must be pointed out that the results of Bates et. al. and Drawin are not, themselves, in agreement. Specifically, the recombination coefficients of Bates et. al. exceed those of Drawin by up to a factor of four while the ionization coefficients are greater by an order of magnitude. At low electron densities, Ne- $10^{16}/cm^3$, our recombination coefficients are generally a factor of one to four less than

those of Drawin and Bates et. al., depending on temperature. At higher Ne, - $10^{18}/cm^3$, our recombination coefficients fall between their results. Our collisional-radiative ionization coefficients are in good agreement (factor of 1.0 - 2.0) with those of Drawin at low Ne, $10^{16}/cm^3$ to $10^{17}/cm^3$. At higher Ne our coefficients exceed those of Drawin by up to a factor of ten. This difference is due primarily to the ionization potential reduction correction discussed above. As a reminder, the calculations of Bates and Drawin are for hydrogen where at higher electron densities the character of the ion does not change. In contrast, in nitrogen other stages of ionization arise.

In a subsequent report it will be shown that the absorption coefficient for our model nitrogen plasma is on the order of $10^4/cm$ in the uv spectral regime. This corresponds to a mean free path of - 10^{-4}cm. In Tables X through XIII the collisional-radiative coefficients are presented for the case where all bound-bound uv lines are assumed to be completely reabsorbed. As expected, there is very little difference between the optically thin and optically thick recombination coefficients. For high electron densities, $\geq 10^{18}/cm^3$, where the plasma is collision-dominant (see the discussion in the next section), the ionization coefficients are comparable. However, for lower electron densities the optically thick ionization coefficients are much larger than the optically thin case, as great as a factor of ten.

C. Saha Equilibrium

When collisional transition rates exceed the corresponding radiative transitions the plasma is said to be collision-dominated. It is then possible to specify the populations of the constituent species by using the Boltzmann-Saha equation at the local electron temperature [11]. The onset of Saha equilibrium depends on Ne and Te; for example, an optically thin nitrogen gas at Te = 1.0 e.v. becomes collision-dominant at Ne - $10^{18}/cm^3$ [5a].

One form of the Saha equation is, [11],

$$\frac{Ne\ N^z(p)}{N^{z-1}(i)} = \frac{2\ g^z(p)}{g^{z-1}(i)} \left\{\frac{mkTe}{2\pi\hbar}\right\}^{3/2} \exp\{-[E^z(p) - E^{z-1}(i)]/kTe\} \qquad (19)$$

We have used eq. (19), after correcting the exponential factor for the ionization potential reduction (see section III. D.), to compare the steady state population densities with those expected assuming a collision-dominant environment for a range of electron densities, Ne = [10^{16} - $10^{19}/cm^3$], and temperatures, Te = [1.0 - 3.0 e.v.]. The ratio of the level population to the Saha population may be defined as

$$\rho^{z-1}(n) = N^{z-1}(n)/N_s^{z-1}(n) \qquad (20)$$

where $N_s^{Z-1}(n)$ is the solution to the corrected eq. (19). In Table XIV we present threshold values for Ne above which $\rho^{Z-1}(n) = 1 \pm .15$ for the indicated levels, i.e. Saha equilibrium is achieved to within 15%. Column 1 requires this criteria to be satisfied for all N I and N II levels, column 2 restricts the criteria to excited states of N I (specifically, i = 7 to 13), and column 3 to excited states of N II (i.e. p = 7 to 17). The results show the following: First, for any given Te, as the number of electrons increases equilibrium is achieved for excited N I states before excited N II states and, as expected, before the lower states. In addition to Ne the threshold values depend on Te. As Te increases more electrons are neccessary to have a completely collision-dominant environment, i.e. complete LTE. For an optically thin nitrogen plasma a state of complete LTE exists if $Ne \geq (2.2 - 5.0) \times 10^{18}/cm^3$ for Te ranging from 1.0 to 3.0 e.v.. The criteria given by Griem [11] and others on the validity of LTE is that the electron deexcitation rate of the resonance line must exceed ten times the radiative decay, i.e. for the nitrogen atom one must have

$$Y(4,1)\ Ne \geq 10\ A(4,1) \qquad (21)$$

For Te = 1.0 e.v., Eq. (21) gives $Ne \geq 2.3 \times 10^{18}/cm^3$ in our case. However, while radiative processes may be important to the lower levels the excited states of N I are still controlled by collisional processes for $Ne \geq (5.7 - 2.1) \times 10^{17}/cm^3$ over the same temperature range. This quasi-stationary state exists for

electron densities four to twenty-five times less than is required for all states to be in LTE.

IV. CONCLUDING REMARKS

The recombination and ionization processes for an optically thin, homogeneous, charge neutral nitrogen plasma have been studied for electron densities between $10^{16}/cm^3$ and $10^{19}/cm^3$ and electron temperatures from 1.0 .ev. to 3.0 e.v.. Effective collisional-radiative recombination and ionization coefficients are calculated which describe the net recombination and ionization and may be used in sophisticated plasma chemistry simulation codes. The bound-bound and free-bound radiation has been characterized. It has been shown that for electron densities greater than $\sim 10^{18}/cm^3$ a state of local thermodynamic equilibrium exists whereas exited states may be in equilibrium, collision-dominant, for electron densities as low as $\sim 10^{17}/cm^3$. This has implications for simplifying the description of radiative transfer in a plasma. For example, above $Ne \sim 10^{18}/cm^3$ a transfer theory based on the assumption of LTE should be adequate while below $Ne \sim 10^{17}/cm^3$ individual species must be considered in detail. In the intermediate regime hybrid theories should prove useful.

TABLE I

Energy Levels for N I

Index	State	Configuration($1s^2 2s^2$)	Energy(e.v.)	Weight
1	$^4S^o$	$2p^3$	0.0	4
2	$^2D^o$	$2p^3$	2.38	10
3	$^2P^o$	$2p^3$	3.58	6
4	^4P	$2p^2(^3P)3s$	10.33	12
5	^2P	$2p^2(^3P)3s$	10.69	6
6	^4P	$2s2p^4$	10.93	12
7	^2S	$2p^2(^3P)3p$	11.60	2
8	^4D	$2p^2(^3P)3p$	11.76	20
9	^4P	$2p^2(^3P)3p$	11.85	12
10	^4S	$2p^2(^3P)3p$	12.00	4
11	^2D	$2p^2(^3P)3p$	12.01	10
12	^2P	$2p^2(^3P)3p$	12.13	6
13	^2D	$2p^2(^1D)3s$	12.36	10

TABLE II

Energy Levels for N II

Index	State	Configuration ($1s^2$)	Energy (e.v.)	Weight
1	^3P	$2s^2 2p^2$	0.01	9
2	^1D	$2s^2 2p^2$	1.90	5
3	^1S	$2s^2 2p^2$	4.05	1
4	$^3D^o$	$2s2p^3$	11.44	15
5	$^3P^o$	$2s2p^3$	13.54	9
6	$^1D^o$	$2s2p^3$	17.88	5
7	$^3P^o$	$2s^2 2p(^2P^o)3s$	18.48	9
8	$^1P^o$	$2s^2 2p(^2P^o)3s$	18.50	3
9	$^3S^o$	$2s2p^3$	19.24	3
10	^1P	$2s^2 2p(^2P^o)3p$	20.41	3
11	^3D	$2s^2 2p(^2P^o)3p$	20.66	15
12	$^1P^o$	$2s2p^3$	20.68	3
13	^3S	$2s^2 2p(^2P^o)3p$	20.94	3
14	^3P	$2s^2 2p(^2P^o)3p$	21.16	9
15	^1D	$2s^2 2p(^2P^o)3p$	21.60	5
16	^1S	$2s^2 2p(^2P^o)3p$	22.10	1
17	$^3F^o$	$2s^2 2p(^2P^o)3d$	23.14	21

TABLE III

Energy Levels for N III

Index	State	Configuration ($1s^2$)	Energy (e.v.)	Weight
1	$^2P^o$	$2s^2 2p$	0.0	6
2	$^4P^o$	$2s2p^2$	7.1	12

TABLE IV

Radiative Transitions (Bound - Bound)

Wavelength(Å)	#(Weise)	Spectrum	Index	Energy (e.v.)
644.99	3	uv	9+ - 1+	19.23
660.28	5	uv	12+ - 2+	18.79
671.48	7	uv	7+ - 1+	18.48
745.84	6	uv	12+ - 3+	16.63
746.98	8	uv	8+ - 2+	16.60
775.96	4	uv	6+ - 2+	15.99
916.34	2	uv	5+ - 1+	13.54
1085.1	1	uv	4+ - 1+	11.43
1134.6	1	uv	4 - 1	10.93
1199.9	2	uv	6 - 1	10.34
1243.3	5	uv	13 - 2	9.98
1411.9	6	uv	13 - 3	8.79
1493.3	3	uv	5 - 2	8.31
1743.6	4	uv	5 - 3	7.12
3437.2	20	near uv	16+ - 8+	3.60
3995.0	19	vis	15+ - 8+	3.10
4623.2	17	vis	14+ - 7+	2.68
5028.8	16	vis	13+ - 7+	2.46
5679.4	15	vis	11+ - 7+	2.18
6482.1	18	vis	10+ - 8+	1.91
7452.2	23	vis	10 - 4	1.66
8211.8	22	ir	9 - 4	1.51
8617.5	25	ir	12 - 5	1.44
8691.6	21	ir	8 - 4	1.43
9395.3	24	ir	11 - 5	1.32
11602.0	7	ir	10 - 6	1.07

TABLE V

Radiative Transitions (Free - Bound Thresholds)

Wavelength(Å)	Spectrum	Index	Energy (e.v.)
413.99	uv	1++ - 1+	29.59
447.58	uv	1++ - 2+	27.70
485.24	uv	1++ - 3+	25.55
490.82	uv	2++ - 4+	25.26
535.32	uv	2++ - 5+	23.16
658.77	uv	2++ - 6+	18.82
710.08	uv	2++ - 9+	17.46
773.91	uv	2++ - 12+	16.02
824.34	uv	4+ - 6	15.04
826.53	uv	3+ - 3	15.00
852.68	uv	1+ - 1	14.54
882.42	uv	2+ - 2	14.05
964.82	uv	2+ - 3	12.85
1019.57	uv	1+ - 2	12.16
1114.93	uv	1++ - 7+	11.15
1116.94	uv	1++ - 8+	11.10
1132.20	uv	1+ - 3	10.96
1349.08	uv	1++ - 10+	9.19
1386.80	uv	1++ - 11+	8.94
1431.64	uv	1++ - 13+	8.66
1468.96	uv	1++ - 14+	8.44
1549.75	uv	1++ - 15+	8.00
1653.07	uv	1++ - 16+	7.50
1919.20	uv	1++ - 17+	6.46
2944.89	uv	1+ - 4	4.21
3046.19	uv	2+ - 13	4.07
3220.26	uv	1+ - 5	3.85
4217.01	vis	1+ - 7	2.94
4459.71	vis	1+ - 8	2.78
4608.92	vis	1+ - 9	2.69
4881.10	vis	1+ - 10	2.54
4900.40	vis	1+ - 11	2.53
5144.40	vis	1+ - 12	2.41

TABLE VI

Collisional-Radiative Recombination Coefficients

Optically Thin (All Wavelengths)

Neutral

Te(e.v.) Ne	1.0	1.5	2.0	2.5	3.0
1.0E+16	2.5E-12	1.1E-12	8.4E-13	5.5E-13	4.6E-13
2.0	2.9	1.5	1.1E-12	8.2	5.4
3.0	3.3	1.8	1.3	1.0E-12	6.5
4.0	3.8	2.2	1.6	1.2	7.6
5.0	4.3	2.6	1.9	1.4	8.8
6.0	4.7	2.9	2.1	1.5	1.0E-12
7.0	5.2	3.3	2.4	1.7	1.1
8.0	5.6	3.7	2.6	1.9	1.2
9.0	6.1	4.0	2.9	2.0	1.3
1.0E+17	6.6	4.3	3.1	2.2	1.5
2.0	1.1E-11	7.4	5.6	3.9	2.6
3.0	1.7	1.1E-11	8.1	5.8	3.8
4.0	2.2	1.4	1.0E-11	7.5	5.0
5.0	2.7	1.7	1.3	9.4	6.3
6.0	3.2	2.0	1.5	1.1E-11	7.6
7.0	3.8	2.4	1.7	1.3	8.9
8.0	4.3	2.6	2.0	1.5	1.0E-11
9.0	4.8	3.0	2.2	1.7	1.1
1.0E+18	5.4	3.4	2.5	1.9	1.3
2.0	1.1E-10	6.8	4.8	3.8	2.7
3.0	1.6	1.0E-10	7.2	5.8	4.1
4.0	2.2	1.4	9.6	7.7	5.6
5.0	2.7	1.7	1.2E-10	9.6	7.0
6.0	3.3	2.1	1.5	1.1E-10	8.6
7.0	3.8	2.4	1.7	1.3	1.0E-10
8.0	4.4	2.8	2.0	1.5	1.2
9.0	4.9	3.2	2.2	1.7	1.3
1.0E+19	5.5	3.5	2.5	1.9	1.5

TABLE VII

Collisional-Radiative Recombination Coefficients

Optically Thin (All Wavelengths)

Te(e.v.) Ne	Ion 1.0	1.5	2.0	2.5	3.0
1.0E+16	3.6E-12	2.1E-12	1.7E-12	1.3E-12	9.7E-13
2.0	4.6	2.6	2.0	1.6	1.1E-12
3.0	5.3	3.1	2.4	1.8	1.3
4.0	5.9	3.6	2.8	2.1	1.4
5.0	6.4	4.1	3.1	2.3	1.6
6.0	6.9	4.6	3.5	2.5	1.7
7.0	7.4	5.0	3.8	2.8	1.9
8.0	8.0	5.5	4.2	3.0	2.0
9.0	8.5	6.0	4.5	3.2	2.2
1.0E+17	9.0	6.4	4.8	3.5	2.3
2.0	1.5E-11	1.0E-11	8.1	5.8	4.0
3.0	2.2	1.5	1.1E-11	8.1	5.8
4.0	2.9	1.9	1.5	1.1E-11	7.4
5.0	3.5	2.3	1.8	1.3	9.2
6.0	4.2	2.7	2.1	1.6	1.1E-11
7.0	4.9	3.2	2.4	1.9	1.3
8.0	5.5	3.6	2.8	2.1	1.5
9.0	6.2	4.0	3.1	2.4	1.7
1.0E+18	6.8	4.5	3.4	2.6	1.9
2.0	1.4E-10	8.9	6.4	5.2	3.9
3.0	2.1	1.3E-10	9.8	7.9	5.9
4.0	2.8	1.8	1.3E-10	1.1E-10	7.9
5.0	3.5	2.2	1.7	1.3	9.9
6.0	4.2	2.7	2.0	1.6	1.2E-10
7.0	4.9	3.1	2.3	1.8	1.4
8.0	5.5	3.6	2.7	2.1	1.6
9.0	6.2	4.0	3.0	2.3	1.8
1.0E+19	6.9	4.5	3.3	2.6	2.0

TABLE VIII

Collisional-Radiative Recombination Coefficients

Optically Thin (All Wavelengths)

Neutral

Te(e.v.) Ne	1.0	1.5	2.0	2.5	3.0
1.0E+16	4.1E-14	4.0E-12	2.2E-11	2.2E-10	4.5E-10
2.0	5.4	5.8	7.0	2.8	6.0
3.0	6.4	7.6	8.8	3.5	7.4
4.0	7.2	9.2	1.0E-10	4.1	8.6
5.0	7.9	1.1E-11	1.2	4.6	9.8
6.0	8.6	1.2	1.3	5.1	1.1E-09
7.0	9.2	1.3	1.5	5.6	1.2
8.0	9.7	1.4	1.6	6.0	1.3
9.0	1.0E-13	1.5	1.7	6.4	1.4
1.0E+17	1.1	1.6	1.8	6.7	1.4
2.0	1.5	2.1	2.4	9.0	2.0
3.0	1.9	2.4	2.8	1.0E-09	2.3
4.0	2.1	2.7	3.0	1.1	2.5
5.0	2.3	2.9	3.2	1.2	2.7
6.0	2.5	3.1	3.3	1.3	2.9
7.0	2.6	3.2	3.4	1.3	3.0
8.0	2.7	3.3	3.5	1.4	3.1
9.0	2.8	3.4	3.6	1.4	3.1
1.0E+18	2.9	3.5	3.7	1.4	3.2
2.0	3.5	4.0	4.1	1.5	3.6
3.0	4.0	4.2	4.3	1.6	3.7
4.0	4.3	4.4	4.4	1.6	3.8
5.0	4.5	4.5	4.5	1.7	3.9
6.0	4.7	4.7	4.6	1.7	4.0
7.0	4.9	4.9	4.6	1.7	4.0
8.0	5.1	5.0	4.7	1.7	4.0
9.0	5.3	5.1	4.8	1.8	4.1
1.0E+19	5.5	5.2	4.8	1.8	4.1

TABLE IX

Collisional-Radiative Ionization Coefficients

Optically Thin (All Wavelengths)

Te(e.v.) Ne	Ion 1.0	1.5	2.0	2.5	3.0
1.0E+16	2.9E-21	4.0E-17	5.8E-15	1.1E-13	8.4E-13
2.0	3.9	5.5	6.8	1.5	1.0E-12
3.0	4.9	7.2	1.0E-14	1.8	1.2
4.0	5.8	9.2	1.3	2.2	1.4
5.0	6.6	1.1E-16	1.5	2.6	1.6
6.0	7.4	1.3	1.8	3.0	1.8
7.0	8.1	1.5	2.0	3.4	2.1
8.0	8.8	1.6	2.2	3.7	2.3
9.0	9.5	1.8	2.4	4.1	2.5
1.0E+17	1.0E-20	1.9	2.6	4.4	2.7
2.0	1.7	3.0	4.3	7.4	4.6
3.0	2.2	3.9	5.6	1.0E-12	6.2
4.0	2.6	4.6	6.6	1.2	7.5
5.0	2.9	5.2	7.4	1.4	8.6
6.0	3.2	5.7	8.1	1.5	9.6
7.0	3.4	6.1	8.6	1.6	1.0E-11
8.0	3.6	6.4	9.2	1.7	1.1
9.0	3.8	6.8	9.6	1.8	1.2
1.0E+18	4.0	7.1	1.0E-13	1.9	1.2
2.0	5.4	9.1	1.2	2.4	1.6
3.0	6.5	1.0E-15	1.4	2.6	1.8
4.0	7.5	1.1	1.5	2.8	1.9
5.0	8.4	1.2	1.5	2.9	2.0
6.0	9.0	1.3	1.6	3.0	2.1
7.0	9.5	1.3	1.7	3.1	2.1
8.0	1.0E-19	1.4	1.7	3.2	2.2
9.0	1.1	1.4	1.8	3.3	2.2
1.0E+19	1.2	1.5	1.8	3.3	2.3

TABLE X

Collisional-Radiative Recombination Coefficients

Optically Thick (All UV Bound-Bound Wavelengths)

Neutral

Te(e.v.) Ne	1.0	1.5	2.0	2.5	3.0
1.0E+16	2.6E-12	1.1E-12	8.2E-13	5.4E-13	4.8E-13
2.0	2.9	1.4	1.1E-12	6.7	5.8
3.0	3.3	1.8	1.3	8.0	7.0
4.0	3.8	2.2	1.6	9.4	8.2
5.0	4.3	2.6	1.8	1.1E-12	9.4
6.0	4.7	2.9	2.0	1.3	1.1E-12
7.0	5.1	3.3	2.3	1.4	1.2
8.0	5.6	3.7	2.5	1.6	1.3
9.0	6.1	4.0	2.8	1.8	1.4
1.0E+17	6.6	4.3	3.0	1.9	1.5
2.0	1.1E-11	7.4	5.6	3.6	2.7
3.0	1.7	1.1E-11	8.1	5.4	4.0
4.0	2.2	1.4	1.0E-11	7.3	5.2
5.0	2.7	1.7	1.3	9.1	6.5
6.0	3.2	2.0	1.5	1.1E-11	7.8
7.0	3.8	2.4	1.7	1.3	9.0
8.0	4.3	2.6	2.0	1.5	1.0E-11
9.0	4.8	3.0	2.2	1.7	1.1
1.0E+18	5.4	3.4	2.5	1.9	1.3
2.0	1.1E-10	6.8	4.8	3.8	2.7
3.0	1.6	1.0E-10	7.2	5.8	4.1
4.0	2.2	1.4	9.6	7.7	5.6
5.0	2.7	1.7	1.2E-10	9.6	7.0
6.0	3.3	2.1	1.5	1.1E-10	8.6
7.0	3.8	2.4	1.7	1.3	1.0E-10
8.0	4.4	2.8	2.0	1.5	1.2
9.0	4.9	3.2	2.2	1.7	1.3
1.0E+19	5.5	3.5	2.5	1.9	1.5

TABLE XI

Collisional-Radiative Recombination Coefficients

Optically Thick (All Bound-Bound UV Wavelengths)

Te(e.v.) Ne	Ion 1.0	1.5	2.0	2.5	3.0
1.0E+16	4.4E-12	2.1E-12	1.7E-12	1.1E-12	1.0E-12
2.0	4.6	2.4	1.9	1.3	1.2
3.0	5.1	3.0	2.4	1.5	1.4
4.0	5.6	3.6	2.8	1.7	1.6
5.0	6.2	4.1	3.1	1.9	1.7
6.0	6.8	4.6	3.5	2.1	1.9
7.0	7.4	5.0	3.8	2.4	2.1
8.0	8.0	5.5	4.2	2.6	2.3
9.0	8.5	6.0	4.5	2.8	2.4
1.0E+17	9.0	6.4	4.8	3.0	2.6
2.0	1.5E-11	1.0E-11	8.1	6.3	5.7
3.0	2.2	1.5	1.1E-11	7.7	6.2
4.0	2.9	1.9	1.5	1.0E-11	8.0
5.0	3.5	2.3	1.8	1.3	9.6
6.0	4.2	2.7	2.1	1.6	1.1E-11
7.0	4.9	3.2	2.4	1.8	1.3
8.0	5.5	3.6	2.8	2.1	1.5
9.0	6.2	4.0	3.1	2.4	1.7
1.0E+18	6.8	4.5	3.4	2.6	1.9
2.0	1.4E-10	8.9	6.4	5.2	3.9
3.0	2.1	1.3E-10	9.8	7.9	5.9
4.0	2.8	1.8	1.3E-10	1.1E-10	7.9
5.0	3.5	2.2	1.7	1.3	9.9
6.0	4.2	2.7	2.0	1.6	1.2E-10
7.0	4.9	3.1	2.3	1.8	1.4
8.0	5.5	3.6	2.7	2.1	1.6
9.0	6.2	4.0	3.0	2.3	1.8
1.0E+19	6.9	4.5	3.3	2.6	2.0

TABLE XII

Collisional-Radiative Ionization Coefficients

Optically Thick (All Bound-Bound UV Wavelengths)

Neutral

Te(e.v.) Ne	1.0	1.5	2.0	2.5	3.0
1.0E+16	3.6E-13	2.0E-11	1.6E-10	4.1E-10	1.0E-09
2.0	3.3	2.2	1.8	5.0	1.2
3.0	3.2	2.4	2.0	5.6	1.4
4.0	3.1	2.7	2.2	6.2	1.5
5.0	3.1	2.8	2.3	6.6	1.6
6.0	3.1	3.0	2.5	7.0	1.7
7.0	3.1	3.0	2.6	7.5	1.8
8.0	3.1	3.1	2.7	8.0	1.9
9.0	3.1	3.2	2.8	8.3	2.0
1.0E+17	3.1	3.2	2.9	8.7	2.0
2.0	3.1	3.4	3.4	1.1E-09	2.5
3.0	3.2	3.5	3.6	1.2	2.8
4.0	3.3	3.6	3.7	1.3	3.0
5.0	3.4	3.7	3.8	1.4	3.1
6.0	3.4	3.8	3.9	1.4	3.2
7.0	3.5	3.8	3.9	1.5	3.2
8.0	3.5	3.9	4.0	1.5	3.3
9.0	3.6	3.9	4.0	1.5	3.3
1.0E+18	3.6	4.0	4.0	1.5	3.4
2.0	4.0	4.3	4.2	1.6	3.6
3.0	4.3	4.5	4.4	1.7	3.8
4.0	4.5	4.6	4.5	1.7	3.9
5.0	4.7	4.7	4.6	1.7	4.0
6.0	4.9	4.9	4.7	1.7	4.1
7.0	5.1	5.0	4.8	1.8	4.1
8.0	5.3	5.1	4.8	1.8	4.1
9.0					
1.0E+19	5.6	5.3	4.9	1.8	4.2

TABLE XIII

Collisional-Radiative Ionization Coefficients

Optically Thick (All Bound-Bound UV Wavelengths)

Te(e.v.) Ne	Ion 1.0	1.5	2.0	2.5	3.0
1.0E+16	4.0E-20	4.9E-16	6.8E-14	1.0E-12	6.7E-12
2.0	4.1	5.3	7.5	1.1	7.6
3.0	4.4	5.8	8.1	1.2	8.2
4.0	4.8	6.2	8.6	1.3	8.9
5.0	5.1	6.5	9.0	1.4	9.5
6.0	5.4	6.8	9.4	1.4	9.9
7.0	5.6	7.0	9.7	1.5	1.0E-11
8.0	5.9	7.1	9.9	1.6	1.1
9.0	6.1	7.2	1.0E-13	1.6	1.1
1.0E+17	6.4	7.3	1.0	1.7	1.1
2.0	8.4	7.8	1.1	2.0	1.4
3.0	1.0E-19	8.2	1.2	2.1	1.6
4.0	1.2	8.4	1.2	2.3	1.7
5.0	1.3	8.6	1.3	2.4	1.7
6.0	1.4	8.8	1.3	2.4	1.8
7.0	1.5	8.9	1.3	2.5	1.9
8.0	1.5	9.1	1.3	2.5	1.9
9.0	1.6	9.2	1.3	2.6	1.9
1.0E+18	1.7	9.4	1.3	2.6	2.0
2.0	2.1	1.0E-15	1.5	2.8	2.2
3.0	2.4	1.1	1.5	3.0	2.3
4.0	2.7	1.2	1.6	3.1	2.3
5.0	3.1	1.3	1.6	3.1	2.4
6.0	3.4	1.3	1.6	3.2	2.4
7.0	3.6	1.4	1.7	3.2	2.5
8.0	3.9	1.4	1.8	3.3	2.5
9.0	4.2	1.5	1.8	3.4	2.5
1.0E+19	4.5	1.5	1.8	3.4	2.5

TABLE XIV

Saha Threshold Values ($/cm^3$)

Te(e.v.)	All states	N(i) ($i \geq 7$)	$N^+(p)$ ($p \geq 7$)
1.0	2.2E+18	4.5E+17	6.4E+17
1.5	2.5E+18	3.6E+17	6.8E+17
2.0	2.9E+18	3.0E+17	7.5E+17
2.5	3.4E+18	2.4E+17	7.8E+17
3.0	* 3.9E+18	* 2.0E+17	8.2E+17

* Excluding N(13)

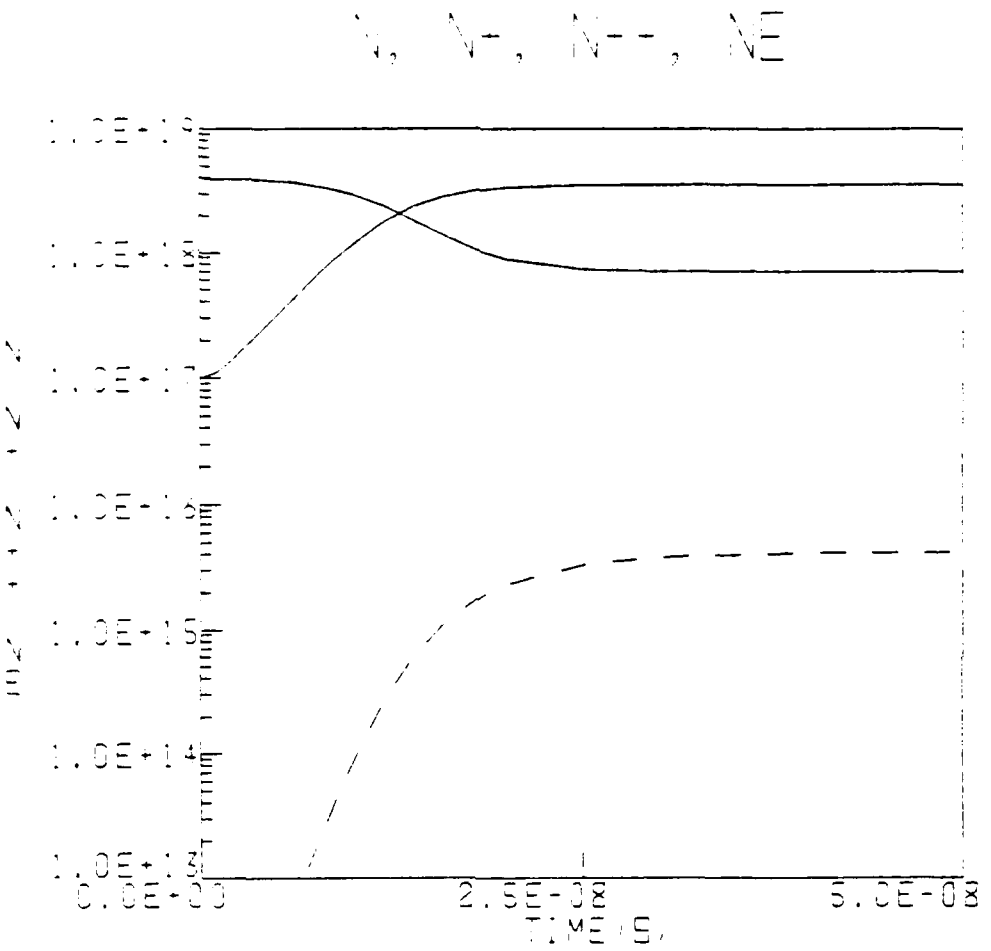

Figure 1.

Population densities for N (solid line, top at t=0), N^+ (solid line, bottom at t=0), N^{--} dashed line), and Ne (same as N^-). All figures are for Te=2.0 e.v.

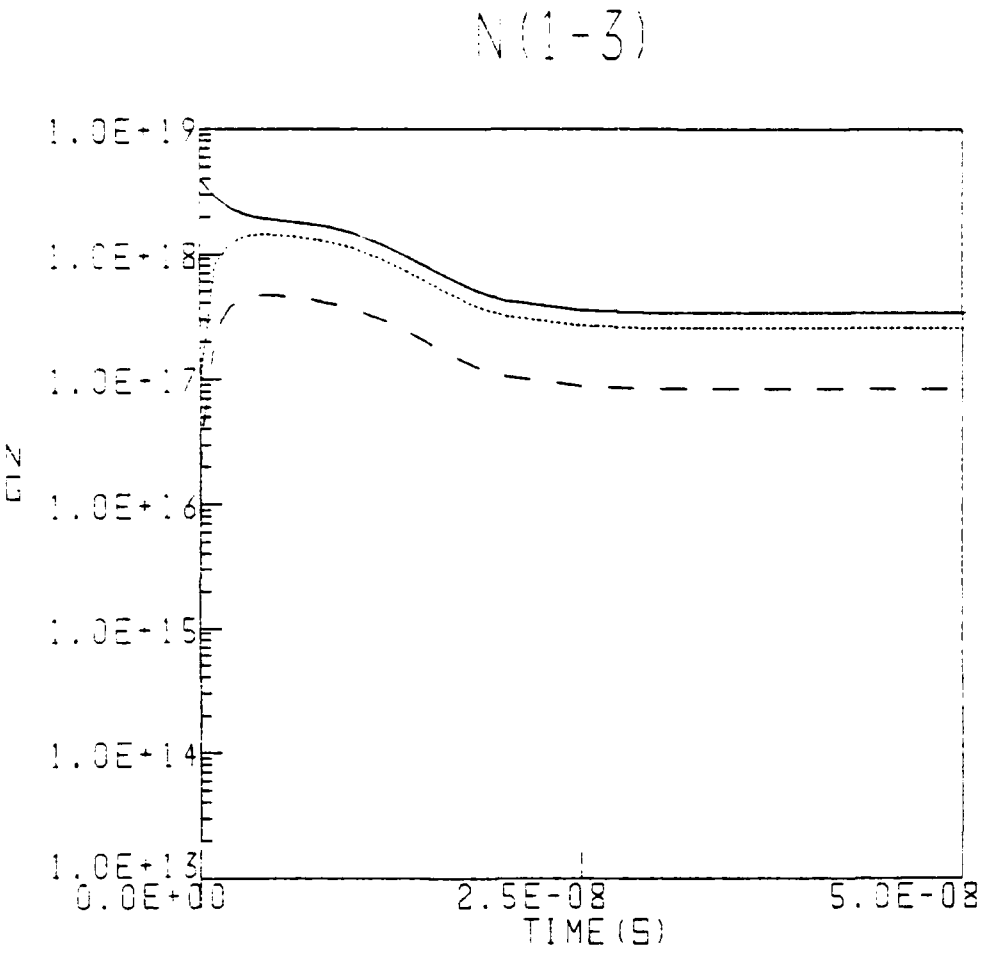

Figure 2.

Population densities for N(1), N(2), and N(3) (solid, dotted, and dashed lines, respectively).

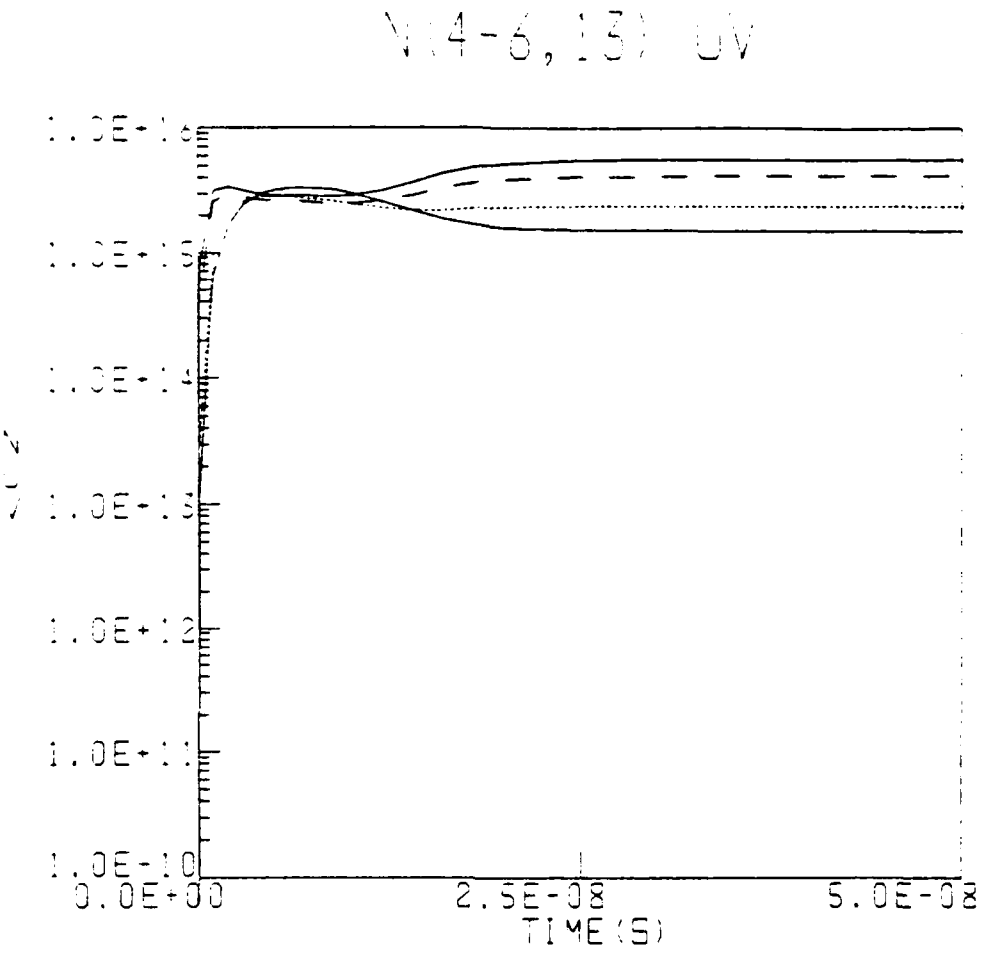

Figure 3.

Population densities for uv emitting N states; i.e. N(4) (solid line, top), N(5) (dotted line), N(6) (dashed line), and N(13) (solid line, bottom).

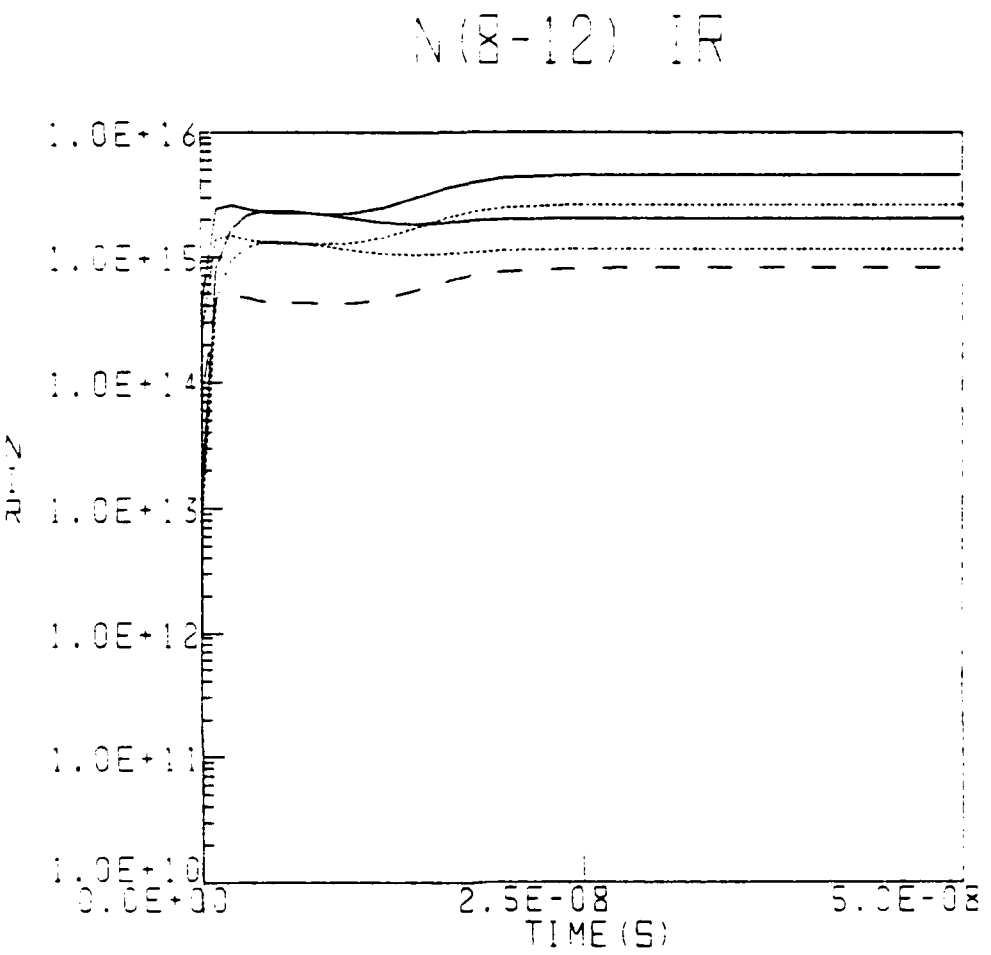

Figure 4.

Population densities for ir emitting N states; i.e. N(8) (solid line, top), N(9) (dotted line, top), N(10) (dashed line), N(11) (solid line, bottom), and N(12) (dotted line, bottom).

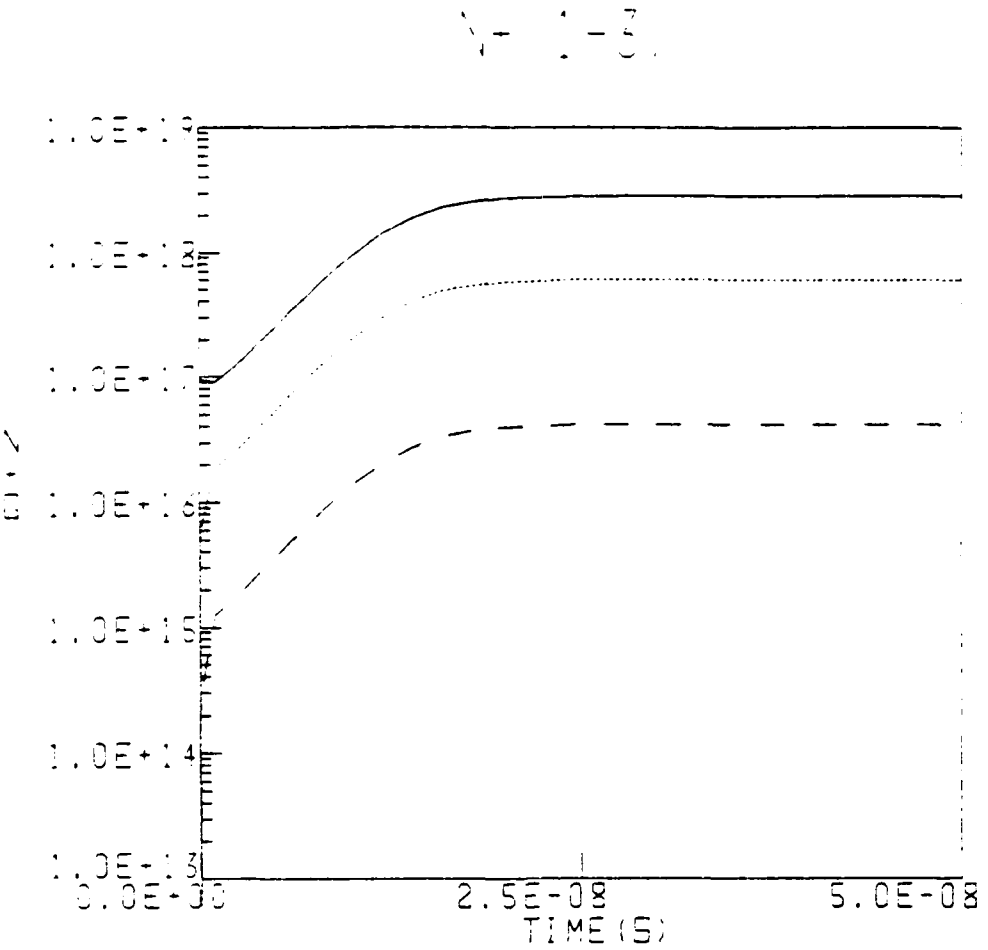

Figure 5.

Population densities for N^+ ground configurations; $N^+(1)$ (solid line), $N^+(2)$ (dotted line), and $N^+(3)$ (dashed line).

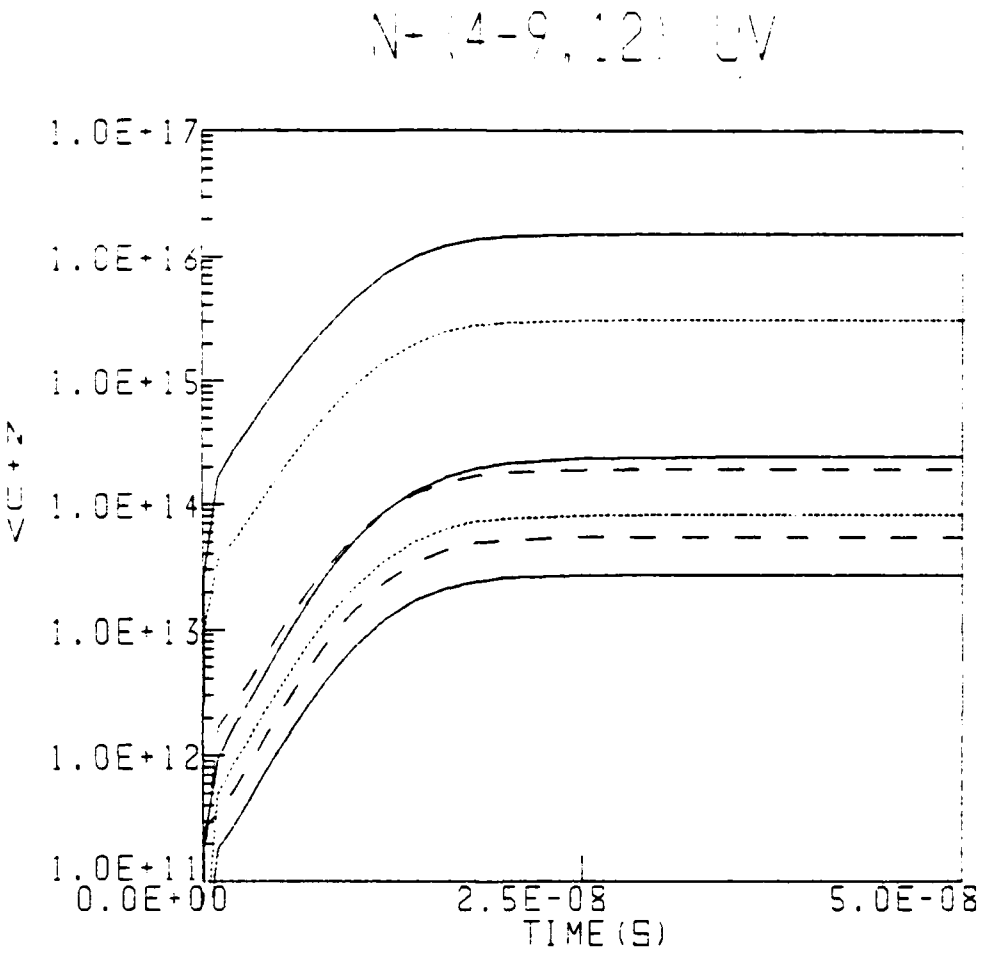

Figure 6.

Population densities for N^+ uv emitting states; $N^+(4)$ (solid line, top), $N^+(5)$ (dotted line, top), $N^+(6)$ (dashed line, top), $N^+(7)$ (solid line, middle), $N^+(8)$ (dotted line, bottom), $N^+(9)$ (dashed line, bottom), and $N^+(12)$ (solid line, bottom).

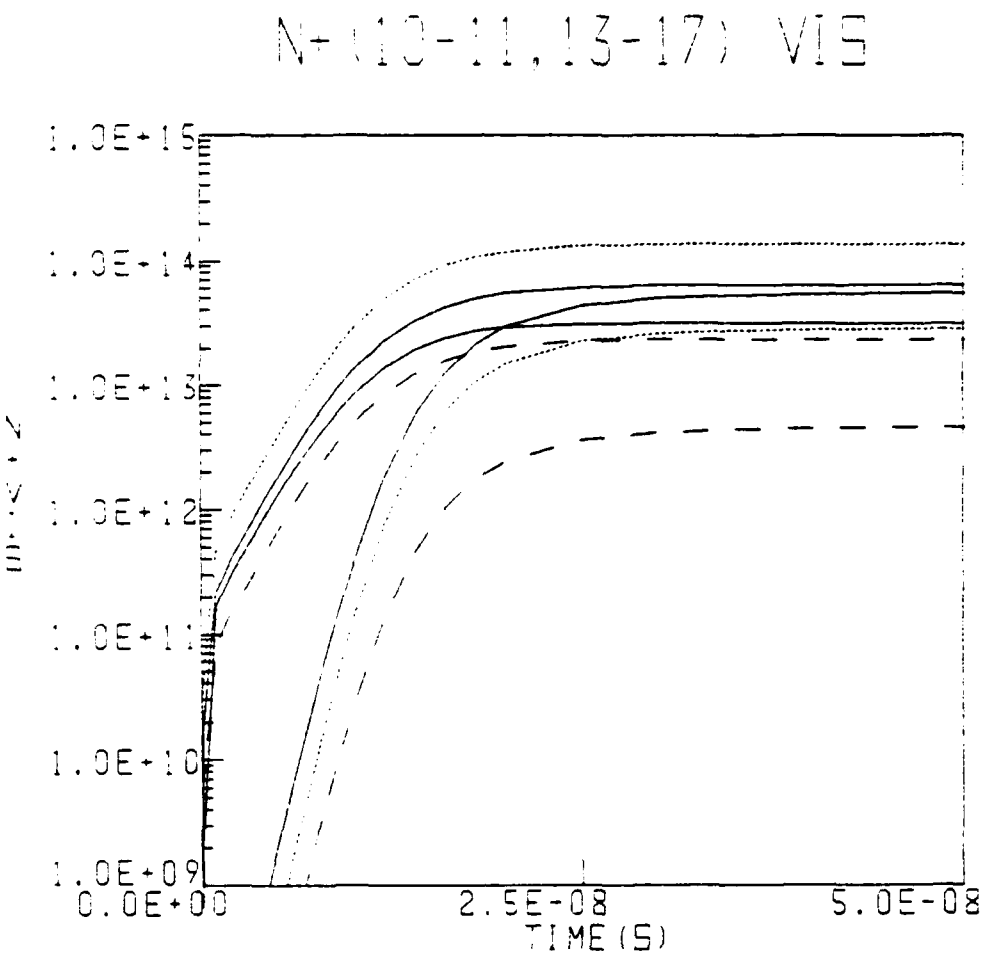

Figure 7.

Population densities for visible emitting N^+ states; final order from top to bottom is $N^+(11)$, $N^+(10)$, $N^+(17)$, $N^+(14)$, $N^+(15)$, $N^+(13)$, and $N^+(16)$.

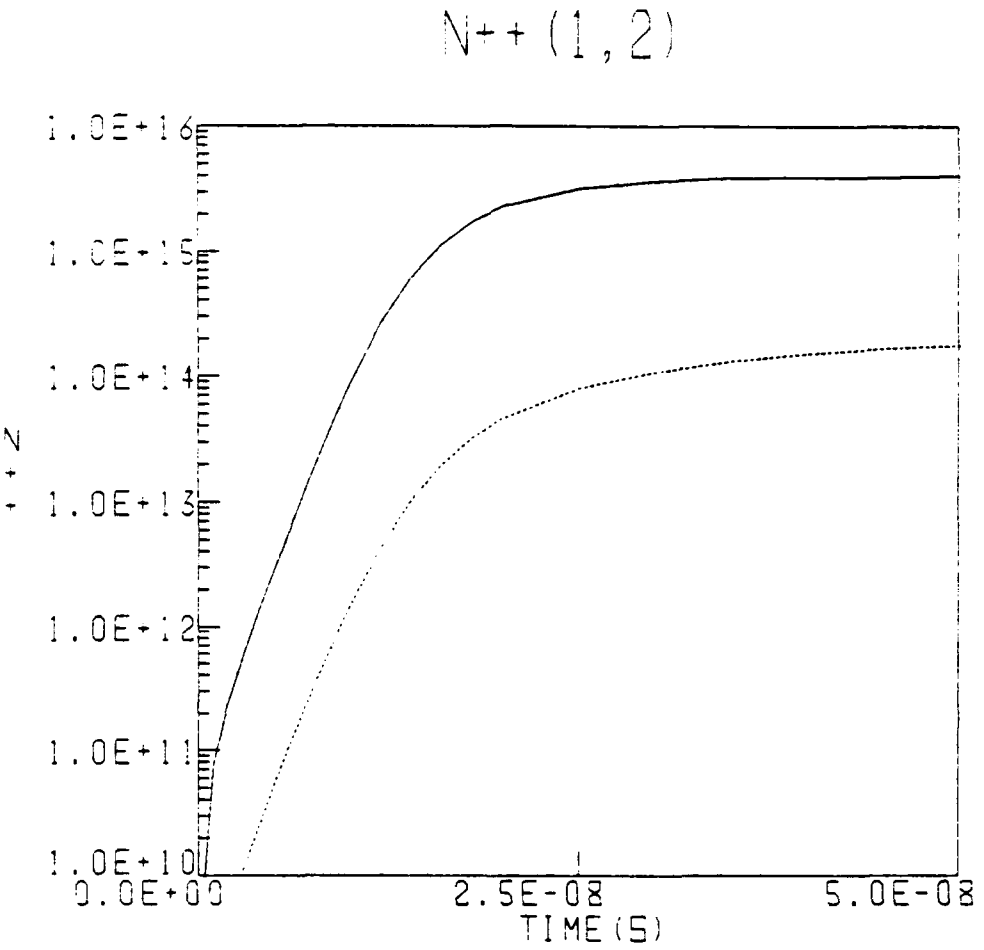

Figure 8.

Population densities for N^{++} levels; $N^{++}(1)$ (solid line) and $N^{++}(2)$ (dotted line).

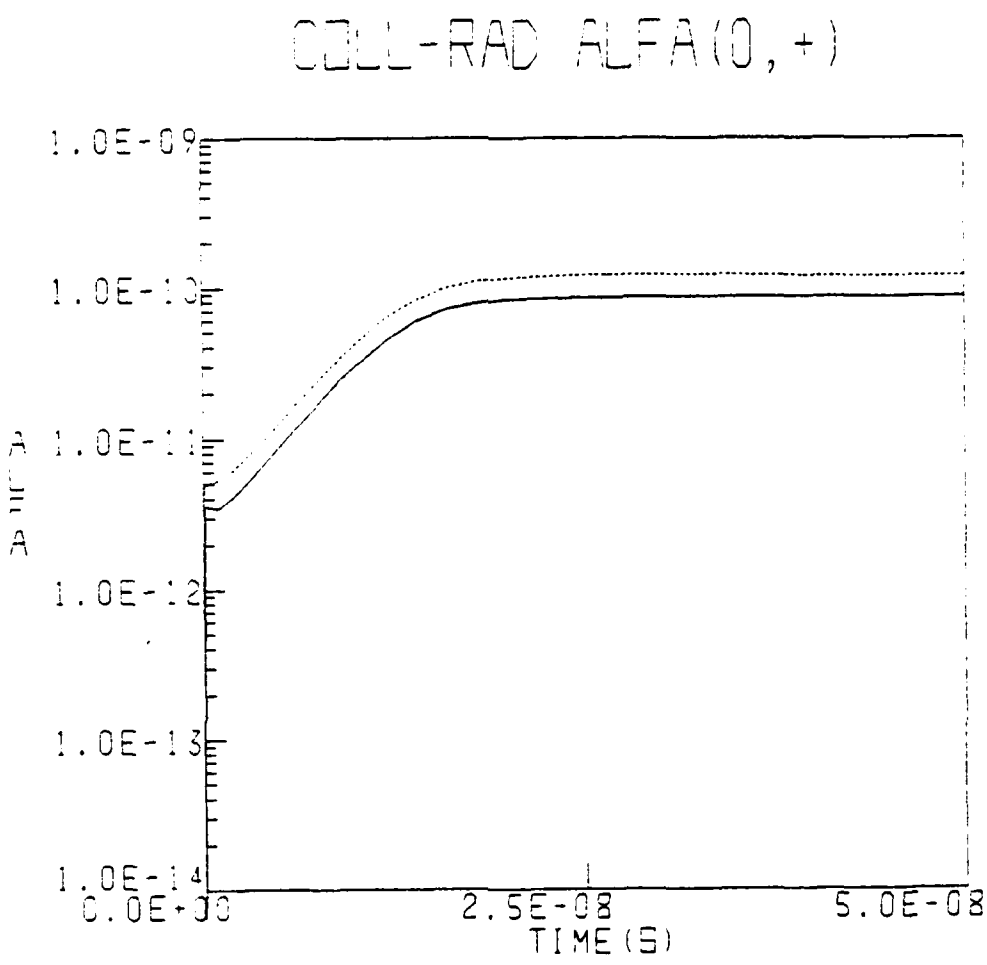

Figure 9.

Collisional-radiative recombination coefficients for optically thin neutral (solid line) and ion (dotted line) cases.

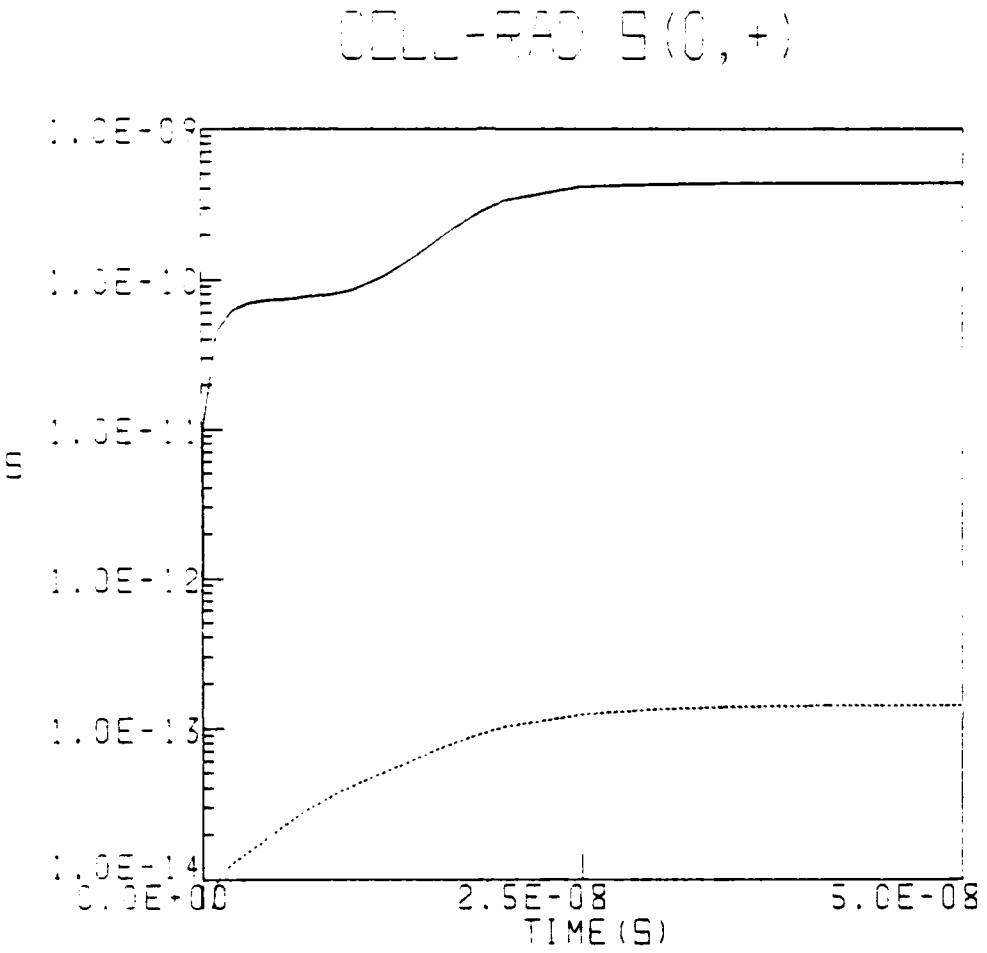

Figure 10.

Collisional-radiative ionization coefficients for the optically thin neutral (solid line) and ion (dotted line) cases.

REFERENCES

1. See for example, Y.B. Zeldovich and Y.P. Raiser, "Physics of Shock Waves and High-Temperature Hydrodynamic Phenomenon" - Vol I, Academic Press, New York (1966)

2. a. D.R. Bates, A.E. Kingston, and R.W.P. McWhirter, Proc. Roy. Soc. A267, 297 (1962).

   b. ibid. A270, 155 (1962).

   c. D.R. Bates and A.E. Kingston, Planet Space Sci. 11, 1 (1963).

   d. D.R. Bates and A. Dalgarno, in Atomic and Molecular Processes, D.R. Bates, ed. Academic Press, New York (1962).

   e. D.R. Bates and A.E. Kingston, Proc. Roy. Soc. A279, 10 (1964).

   f. ibid. 32 (1964).

3. a. H.W. Drawin, Z. Physik 225, 470 (1969).

   b. ibid. 483 (1969).

4. C. Park, J. Quant. Spectrosc. Radiat. Transfer 8, 1633 (1968).

5. a. J.L. Kulander, J. Quant. Spectrosc. Radiat. Transfer 5, 253 (1965).

   b. ibid. 6, 31 (1966).

6. A.W. Ali and W.W. Jones, Physics Letters 55A, 462(1976) and W.W. Jones and A.W. Ali, Appl. Phys. Letters 26 450(1975).

7. W.L. Weise, M.W. Smith, and B.M. Glennon, Atomic Transition Probabilities, NBS Publication #NSRDS-NBS4, (1966).

8. A.W. Ali, R.H. Kummler, F.R. Gilmore, and J. William McGowan, "Upper Atmospheric Excitation Processes", NRL Memorandum Report 3920 (1979). ADA067330

9. H.W. Drawin, "Collision and Transport Cross Sections", Report EUR-CEA-FC-383, Fontenay-aux-Roses, 1966 Revised (1967).

10. S. Slinker and A.W. Ali, "Electron Excitation and Ionization Rate Coefficients For N_2, O_2, NO, N, and O", NRL Memorandum Report 4756 (1982). ADA110988

11. H. Griem, Plasma Spectroscopy, McGraw-Hill Book Co., New York (1964).

12. T.R. Young, "CHEMEQ - A Subroutine for Solving Stiff Ordinary Differential Equations", NRL Memorandum Report 4091 (1980). ADA083545

DISTRIBUTION LIST

Chief of Naval Operations
Washington, DC 20350
ATTN: Dr. C. F. Sharn (OP09873)

U. S. Army Ballistics Research Laboratory
Aberdeen Proving Ground, Maryland 21005
ATTN: Dr. Donald Eccleshall (DRXBR-BM)
Dr. Anand Prakash

Office of Under Secretary of Defense
Research and Engineering
Room 3E1034
The Pentagon
Washington, DC 20301
ATTN: Mr. John M. Bachkosky

Office of Naval Research
800 North Quincy Street
Arlington, VA 22217
ATTN: Dr. C. W. Roberson

Chief of Naval Material
Office of Naval Technology
MAT-0712, Room 503
800 North Quincy Street
Arlington, VA 22217
ATTN: Dr. Eli Zimet

Commander
Naval Sea Systems Command
PMS-405
Washington, DC 20362
ATTN: CAPT R. Topping
CDR W. Bassett

Air Force Office of Scientific Research
Physical and Geophysical Sciences
Bolling Air Froce Base
Washington, DC 20332
ATTN: CAPT Henry L. Pugh, Jr.

Department of Energy
Washington, DC 20545
ATTN: Dr. Terry F. Godlove (ER20:GTN, High Energy and Nuclear Physics)
Dr. James E. Leiss (G-256)
Mr. Gerald J. Peters (G-256)

Joint Institute for Laboratory Astrophysics
National Bureau of Standards and
University of Colorado
Boulder, CO 80309
ATTN: Dr. Arthur V. Phelps

Lawrence Berkeley Laboratory
University of California
Berkeley, CA 94720
ATTN: Dr. Edward P. Lee

Ballistic Missile Defense Advanced Technology Center
P.O. Box 1500
Huntsville, AL 35807
ATTN: Dr. M. Hawie (BMDSATC-1)

Intelcom Rad Tech.
P.O. Box 81087
San Diego, CA 92138
ATTN: Dr. W. Selph

Lawrence Livermore National Laboratory
University of California
Livermore, CA 94550
ATTN: Dr. Richard J. Briggs
Dr. Thomas Fessenden
Dr. Frank Chambers
Dr. James W.-K. Mark, L-477
Dr. William Fawley
Dr. William Barletta
Dr. William Sharp
Dr. Daniel S. Prono
Dr. John K. Boyd
Dr. Kenneth W. Struve
Dr. John Clark
Dr. George J. Caporaso
Dr. William E. Martin
Dr. Donald Prosnitz
Dr. S. Yu

Mission Research Corporation
735 State Street
Santa Barbara, CA 93102
ATTN: Dr. C. Longmire
Dr. N. Carron

National Bureau of Standards
Gaithersburg, MD 20760
ATTN: Dr. Mark Wilson

Science Applications, Inc.
1200 Prospect Street
La Jolla, CA 92037
ATTN: Dr. M. P. Fricke
Dr. W. A. Woolson

Science Applications, Inc.
5 Palo Alto Square, Suite 200
Palo Alto, CA 94304
ATTN: Dr. R. R. Johnston
Dr. Leon Feinstein
Dr. Douglas Keeley

Science Applications, Inc.
1651 Old Meadow Road
McLean, VA 22101
ATTN: Mr. W. Chadsey

Naval Surface Weapons Center
White Oak Laboratory
Silver Spring, MD 20910
ATTN: Mr. R. J. Biegalski
Dr. R. Cawley
Dr. J. W. Forbes
Dr. D. L. Love
Dr. C. M. Huddleston
Dr. G. E. Hudson
Mr. W. M. Hinckley
Mr. N. E. Scofield
Dr. E. C. Whitman
Dr. M. H. Cha
Dr. H. S. Uhm
Dr. R. Fiorito
Dr. H. C. Chen

C. S. Draper Laboratories
Cambridge, MA 02139
ATTN: Dr. E. Olsson
Dr. L. Matson

Physcal Dynamics, Inc.
P.O. Box 1883
La Jolla, CA 92038
ATTN: Dr. K. Brueckner

Avco Everett Research Laboratory
2385 Revere Beach Pkwy
Everett, MA 02149
ATTN: Dr. R. Patrick
Dr. Dennis Reilly
Dr. D. H. Douglas-Hamilton

Defense Technical Information Center
Cameron Station
5010 Duke Street
Alexandria, VA 22314 (2 copies)

Naval Research Laboratory
Washington, DC 20375
ATTN: M. Lampe - Code 4792
M. Friedman - Code 4700.1
J. R. Greig - Code 4763
I. M. Vitkovitsky - Code 4701
J. B. Aviles - Code 6650
M. Haftel - Code 6651
T. Coffey - Code 1001
S. Ossakow - Code 4700 (26 copies)
P. Sprangle - Code 4790
Library - Code 2628 (20 copies)
A. W. Ali - Code 4700.1 (30 copies)
D. Book - Code 4040
J. Boris - Code 4040
R. Hubbard - Code 4790
B. Hui - Code 4790
S. Slinker - Code 4790
G. Joyce - Code 4790
D. Murphy - Code 4763
A. Robson - Code 4760
D. Colombant - Code 4790
M. Picone - Code 4040
M. Raleigh - Code 4763
R. Pechacek - Code 4763
G. Cooperstein - Code 4770
Y. Lau - Code 4790
R. Fernsler - Code 4790

Defense Advanced Research Projects Agency
1400 Wilson Blvd.
Arlington, VA 22209
ATTN: Dr. S. Shey

Physics International, Inc.
2700 Merced Street
San Leanadro, CA 94577
ATTN: Dr. E. Goldman

SDIO - DEW
Office of Secretary of Defense
Washington, DC 20301
ATTN: Lt. Col. R. L. Gullickson

Mission Research Corp.
1720 Randolph Road, S.E.
Albuquerque, NM 87106
ATTN: Dr. Brendan Godfrey
Dr. Richard Adler
Dr. Thomas Hughes
Dr. Lawrence Wright

Princeton University
Plasma Physics Laboratory
Princeton, NJ 08540
ATTN: Dr. Francis Perkins, Jr.

McDonnell Douglas Research Laboratories
Dept. 223, Bldg. 33, Level 45
Box 516
St. Louis, MO 63166
ATTN: Dr. Evan Rose
Dr. Carl Leader

Cornell University
Ithaca, NY 14853
ATTN: Prof. David Hammer

Sandia National Laboratory
Albuquerque, NM 87115
ATTN: Dr. Bruce Miller
Dr. Barbara Epstein
Dr. John Freeman
Dr. John E. Brandenburg
Dr. Gordon T. Leifeste
Dr. Carl A. Ekdahl, Jr.
Dr. Gerald N. Hays
Dr. James Chang
Dr. Michael G. Mazerakis

University of California
Physics Department
Irvine, CA 92664
ATTN: Dr. Gregory Benford

Air Force Weapons Laboratory
Kirtland Air Force Base
Albuquerque, NM 87117
ATTN: D. Straw (AFWL/NTYP)
C. Clark (AFWL/NTYP)
W. Baker (AFWL/NTYP)
D. Dietz (AFWL/NTYP)
Lt Col J. Head

Pulse Sciences, Inc.
14796 Wicks Blvd.
San Leandro, CA 94577
ATTN: Dr. Sidney Putnam
Dr. John Bayless

Los Alamos National Scientific Laboratory
P.O. Box 1663
Los Alamos, NM 87545
ATTN: Dr. L. Thode
Dr. A. B. Newberger, X-3, MS-608
Dr. M. A. Mostrom, MS-608
Dr. T. P. Starke, MS-942
Dr. H. Dogliani, MS-5000

Institute for Fusion Studies
University of Texas at Austin
RLM 11.218
Austin, TX 78712
ATTN: Prof. Marshall N. Rosenbluth

University of Michigan
Dept. of Nuclear Engineering
Ann Arbor, MI 48109
ATTN: Prof. Terry Kammash
Prof. R. Gilgenbach

Directed Technologies, Inc.
226 Potomac School Road
McLean, VA 22101
ATTN: Dr. Ira F. Kuhn
Dr. Nancy Chesser

Titan Systems, Inc.
8950 Villa La Jolla Drive-Suite 2232
La Jolla, CA 92037
ATTN: Dr. H. L. Buchanon
Dr. R. M. Dowe

Lockheed Palo Alto Laboratory
3251 Hanover Street
Bldg. 203, Dept. 52-11
Palo Alto, CA 94304
ATTN: Dr. John Siambis

University of Maryland
Physics Department
College Park, MD 20742
ATTn: Dr. Y. C. Lee
Dr. C. Grebogi

Science Applications, Inc.
1710 Goodridge Dr.
McLean, VA 22102
ATTN: Dr. A. Drobot
Dr. K. Papadopoulos

Dr. Jonn P. Jackson
Kaman Sciences
1500 Garden of the Gods Road
Colorado Springs, CO 80933

DASIAC - DETIR
Kaman Tempo
25600 Huntington Avenue, Suite 500
Alexandria, VA 22303
ATTN: Mr. F. Wimenitz

Director of Research
U.S. Naval Academy
Annapolis, MD 21402 (2 copies)

END

FILMED

7-85

DTIC